ADVANCED ELECTRONIC MATERIALS
www.advelectronicmat.de

Ultrathin, Breathable, Permeable, and Skin-Adhesive Charge Storage Electronic Tattoos Based on Biopolymer Nanofibers and Carbon Nanotubes

*Shalik Ram Joshi, Ajay Pratap, Narendar Gogurla, and Sunghwan Kim**

Ultrathin, breathable, and skin-compatible epidermal electronics are attractive for wearable and implantable healthcare and biomedical applications. However, materializing and integrating all electronic components on ultrathin platforms is still challenging. Here, a charge-storing electronic tattoo (E-tattoo) device with ultrathin, breathable, and skin-compatible properties is reported. Silk protein nanofibers (SNFs) and carbon nanotubes (CNTs) form the top and bottom electrodes that sandwich the intermediate dielectric layer fabricated using poly(vinyl alcohol) nanofibers. The E-tattoo capacitors on the deformed skin, show excellent mechanical and electrical stability, and 60 µm-thick capacitors exhibit frequency-dependent capacitances (up to 350 pF at 5 kHz) and capability for memory operation. Mechanical bending induces capacitance change, which increases as the bending radius is decreased, indicating mechanical sensing capability of the E-tattoo. SNF/CNT-based triboelectric nanogenerator E-tattoos can be connected to the capacitor E-tattoo, and the charges generated by multiple bare-finger touches can be stored in the capacitor (0.23 V for 200 touches). Due to the micro/nanopores in the NF networks, the device exhibits a water vapor transmission rate of 115.04 g m^{-2} d^{-1}, which is better than that of a commercial band-aid, as well as ethanol sensing capability. Developed E-tattoo capacitor can be used for constructing multicomponent integrated ultrathin and epidermal electronics.

1. Introduction

Measuring the electrophysiological signals of organs and tissues is the key approach for healthcare monitoring and for obtaining a better understanding of human functions.[1] Accordingly, ultrathin and flexible electronic devices compatible with soft human skin have remained under the spotlight because of their advantageous properties that facilitate such applications.[2] Recent advances in such skin-compatible thin electronics, sometimes referred to as epidermal electronic tattoo (E-tattoo), have facilitated the realization of conformal interfacing at human skin. Most epidermal E-tattoo electronics have been demonstrated on flexible polymer substrates, including poly(dimethylsiloxane) (PDMS),[3] polyimide,[4] poly (L-lactide-co-glycolide),[5] and poly(ethylene terephthalate),[6] using conventional methods (e.g., high temperature and vacuum processing). However, realizing features such as low costs, biocompatibility, high deformability, and excellent skin-adhesion, that are imperative for biomedical and healthcare applications, is a considerable challenge. For seamless biotic–abiotic interfaces, electronic materials used for E-tattoos must be compatible with highly deformable skins, along with being cost-effective, biocompatible, and skin-adhesive. Nanofibers formed using silk protein, which is a natural protein extracted from *Bombyx mori* cocoons, can be a promising solution to these issues, because silk protein is biocompatible and can be easily functionalized. Therefore, silk nanostructures offer a remarkable platform to implement deformable, skin-adhesive, biocompatible, and functional electronic and photonic devices.[7] Moreover, with the advantages of mechanical strength and high electrical/thermal conductivities of carbon nanotubes (CNTs), a biocompatible, functionalized, and skin-conformal E-tattoo system can be obtained.[8]

Among various electronic components for on-skin electronics, energy storage devices, such as capacitors and batteries, are becoming increasingly important because of the energy autonomy of on-skin and in-body electrical operations.[9] Additionally, the capacitor form, i.e., two electrode layers sandwiching an intermediate dielectric layer, can provide highly sensitive chemical and motion sensing capabilities, when the dielectric layer is designed to respond to applied analytes and mechanical forces. With such a dielectric layer, the accumulation of carriers (electrons) can enhance the sensitivity of the

S. R. Joshi, S. Kim
Department of Biomedical Engineering & Department of Electronic Engineering
Hanyang University
Seoul 04763, Korea
E-mail: skim81@hanyang.ac.kr
A. Pratap, N. Gogurla
Department of Energy Systems Research
Ajou University
Suwon 16499, Korea

The ORCID identification number(s) for the author(s) of this article can be found under https://doi.org/10.1002/aelm.202201095.

DOI: 10.1002/aelm.202201095

device because of the enhanced carrier–matter interactions.[10] This mechanism is similar to the use of optical cavities for highly sensitive sensing applications based on enhanced light–matter interactions.[11] Recently, self-sustainable batteries and capacitors that are flexible and can be conformally attached onto skin or tissue surfaces have been demonstrated.[12] However, the use of a substrate restricts the flexibility, skin-adhesion, and breathability of these devices, and results in high fabrication costs. For on-skin and in-body operations, the thinnest possible energy storage devices need to be fabricated using cost-effective processes and bio-friendly materials. Further, these devices should exhibit good tissue-adhesion and breathability. Permeability to analytes (which may be in the form of gas, moisture, or liquid) is crucial to enable fast, sensitive, and accurate detection of physiological signals in many health-monitoring applications.[13] In addition to causing discomfort, covering impermeable materials or transdermal devices, especially those that are directly bonded to the skin, can also cause allergic reactions and inflammation.[13]

Here, we report an ultrathin, breathable, and skin-compatible capacitor E-tattoo that was fabricated using silk nanofibers (SNFs), poly(vinyl alcohol) nanofibers (PVANFs), and CNTs. The SNF/CNT conductive layers were used as the top and bottom electrodes, and the PVANF dielectric layer was sandwiched in between them. Because of the inherent micro/nanopores in the NF networks, the capacitor E-tattoo exhibits breathability, permeability, and deformability. Due to the SNFs, the E-tattoo device could be strongly and bio compatibly adhered to human skin, and showed mechanical and electrical stability under various mechanical deformations applied to the E-tattoo-attached skin. Moreover, the fabricated E-tattoo exhibited charge storing capability, which was evident from the observed frequency-dependent capacitance (up to 350 pF at 5 kHz) and closed loops in the capacitance–voltage (C–V) curves of the E-tattoo. Additionally, the charge generation was found to be enhanced by increasing the temperature. Deformation of the insulator layer by mechanical bending increased the capacitance, indicating the motion sensing capability of the E-tattoo. A CNT and SNF-based E-tattoo was used as a triboelectric nanogenerator (TENG) and connected to the capacitor E-tattoo. We confirmed that finger touches on the TENG led to the generation of charges, which were stored in the capacitor. Furthermore, the water vapor transmission rates (WVTRs) of the E-tattoo devices were better than that of the commercial band-aid, and they also exhibited ethanol (EtOH) sensing capabilities. This work reveals a route to overcome the gap between two contradictory requirements in epidermal electronics, viz. skin-compatibility (ultrathin, deformability, and biocompatibility) and implementation of various functional components on a single platform.

2. Results and Discussion

Figure 1a depicts a schematic illustration of an ultrathin E-tattoo for the charge-storing, breathable, and permeable electrical capacitor produced by SNFs, PVANFs, and CNTs. Details of the fabrication are explained in the Methods section. In brief, first we prepared two thin SNF/CNT E-tattoo layers. The SNF layers were fabricated using the electrospinning method, and then the CNT ink was drawn onto the SNF layers (Experimental Section and Figure S1, Supporting Information). During the drying process, methanol in the CNT ink induced crosslinking in the SNFs, resulting in a water- and solvent-stable NF network. The scanning electron microscopy (SEM) image of the electrospun SNFs in Figure 1 indicates the presence of randomly interconnected fibers (diameter: ≈600 nm) with hierarchical pore structures in the micro-to-nano range (Figure 1b). Fourier transform infrared (FTIR) spectroscopy results showed that β-sheet crystallites (corresponding to the frequency of 1624 cm^{-1}) were generated in the SNF/CNT E-tattoo,[14] and the peaks at 1740 cm^{-1} (−COOH) and 3000 cm^{-1} ($-CH_2$) observed in the FTIR profile could be attributed to CNTs[15] (Figure S2, Supporting Information). In the SNF/CNT E-tattoo, the CNTs were uniformly functionalized on the SNF layer and filled partially into the voids of the SNF networks that resulted in a high electrical conductivity through the E-tattoo (Figure 1c). Thereafter, as an intermediate dielectric layer, a PVANF layer was generated using the electrospinning method (Experimental Section and Figure S3, Supporting Information). The SEM image in Figure 1d reveals that the layer consists of PVANFs with a diameter of 300 nm. Two SNF/CNT layers were placed at the top and bottom of the PVANF layer after spraying EtOH and then mechanically pressed for a few hours to make the capacitor form. In order to investigate the on-skin stability and adhesion of the E-tattoo capacitor, we carried out the peeling test by first affixing an adhesive tape to the skin-attached E-tattoo capacitor, and then removing the tape from the skin after it had been adhered to the skin by the adhesive tape (Figure S4, Supporting Information). The E-tattoo capacitor was successfully used for on-skin monitoring with reliable E-skin adherence after several affixing-peeling tests. As evident from the cross-sectional view of the E-tattoo in Figure 1e, the 18-µm-thick PVANF layer was sandwiched between two 22-µm-thick SNF/CNT layers, and all the layers were bonded to each other with a seamless interface. The E-tattoo with an area of 1 cm^2 had a mass of only 2.3 mg (2.3 mg cm^{-2} as areal density) and was thus much lighter than those used in reported epidermal electronic devices[4a] (Figure S5, Supporting Information). This low weight of the tattoo allows imperceptible tattooing, and the SNFs facilitate a remarkable skin adhesion, biocompatibility at the tattoo–skin interface, breathability, and permeability.

With the advantages of SNFs, skin-tattooing is easily possible via van der Waals bonding between the SNFs and the skin. This boding is induced when the water molecules at the E-tattoo and skin interface are naturally evaporated through the E-tattoo. This method allows conformal integration of the E-tattoo on skin with uneven surfaces (Figure 1f). Under mechanical deformations such as compressing, stretching, and twisting, the E-tattoo was stably preserved with no damage (Figure 1f). To investigate the stability of electrical properties under applied mechanical forces, the SNF/CNT E-tattoo was attached on a pig skin, and an electrical signal was applied. Figure 1i shows the current–voltage (I–V) characteristics of the SNF/CNT E-tattoo attached on the skin. The observed linear relation indicates that the contact was perfectly ohmic (sheet resistance 200 Ω/□), proving the capability of our E-tattoo as an electrical conductor. As expected, the electrical resistances were preserved under

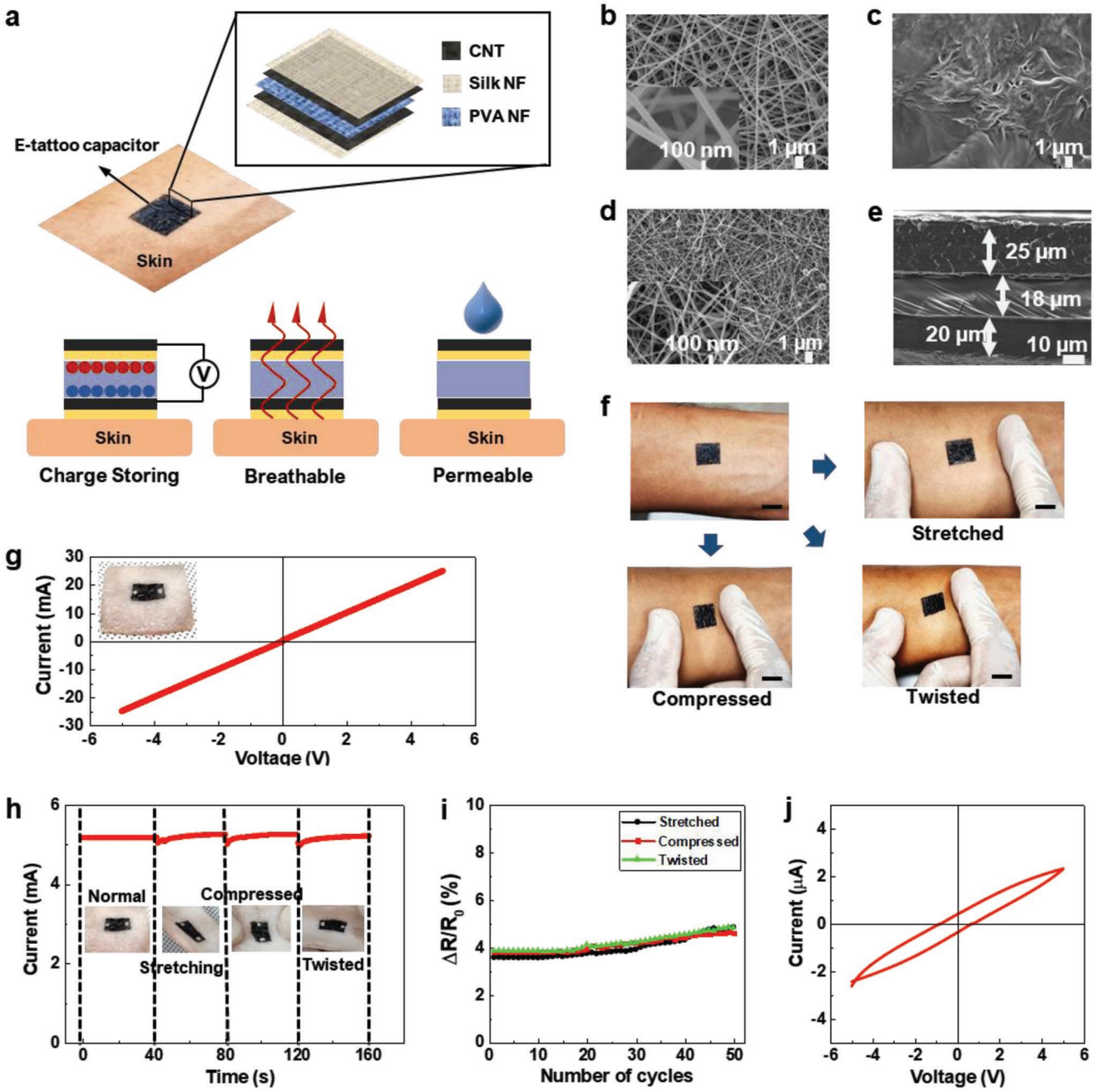

Figure 1. Design of the SNF-CNT/PVA/CNT-SNF capacitor and electrical characteristics of the CNT-SNF-based E-tattoo. a) Schematic illustration and optical image of the SNF-CNT/PVA/CNT-SNF capacitor, with multifunctionalities such as on-skin charge storage, breathability, and permeability, attached to the skin. SEM image of the b) methanol-treated electrospun SNF, c) CNT-functionalized SNF, and d) electrospun PVA nanofibers. e) Cross-sectional SEM image of the SNF-CNT/PVA/CNT-SNF capacitor showing its thickness. f) Optical image demonstrating the stability of the E-tattoo (scale bar is 10 mm), attached to the skin, under mechanical deformation (stretched, compressed and twisted). g) *I–V* curve of the E-tattoo on a pig skin to show the ohmic nature of the electrode. h) Current response and i) mechanical durability of the E-tattoo under different mechanical deformations (stretching, compressing, and twisting). j) Dual sweep *I–V* of the SNF-CNT/PVA/CNT-SNF capacitor demonstrating capacitive effect.

the applied mechanical deformations (Figure 1h). Movement of electrical contacts was the primary cause of a slight change in the twisting-induced current. The electrical current was also stable over fifty mechanical cycles under stretched, compressed, and twisted conditions (Figure 1i). The resistance showed the same value during the twenty cycles. Over the twenty cycles, weak degradation in the resistance could be observed, but the resistance increasement was being constrained by 20%. With two SNF/CNT E-tattoo stickers and a PVANF layer, a functional E-tattoo component was built, which could store the generated electrical energy (Figure 1j). The stable electrical properties of the skin-attached E-tattoo, as demonstrated under various

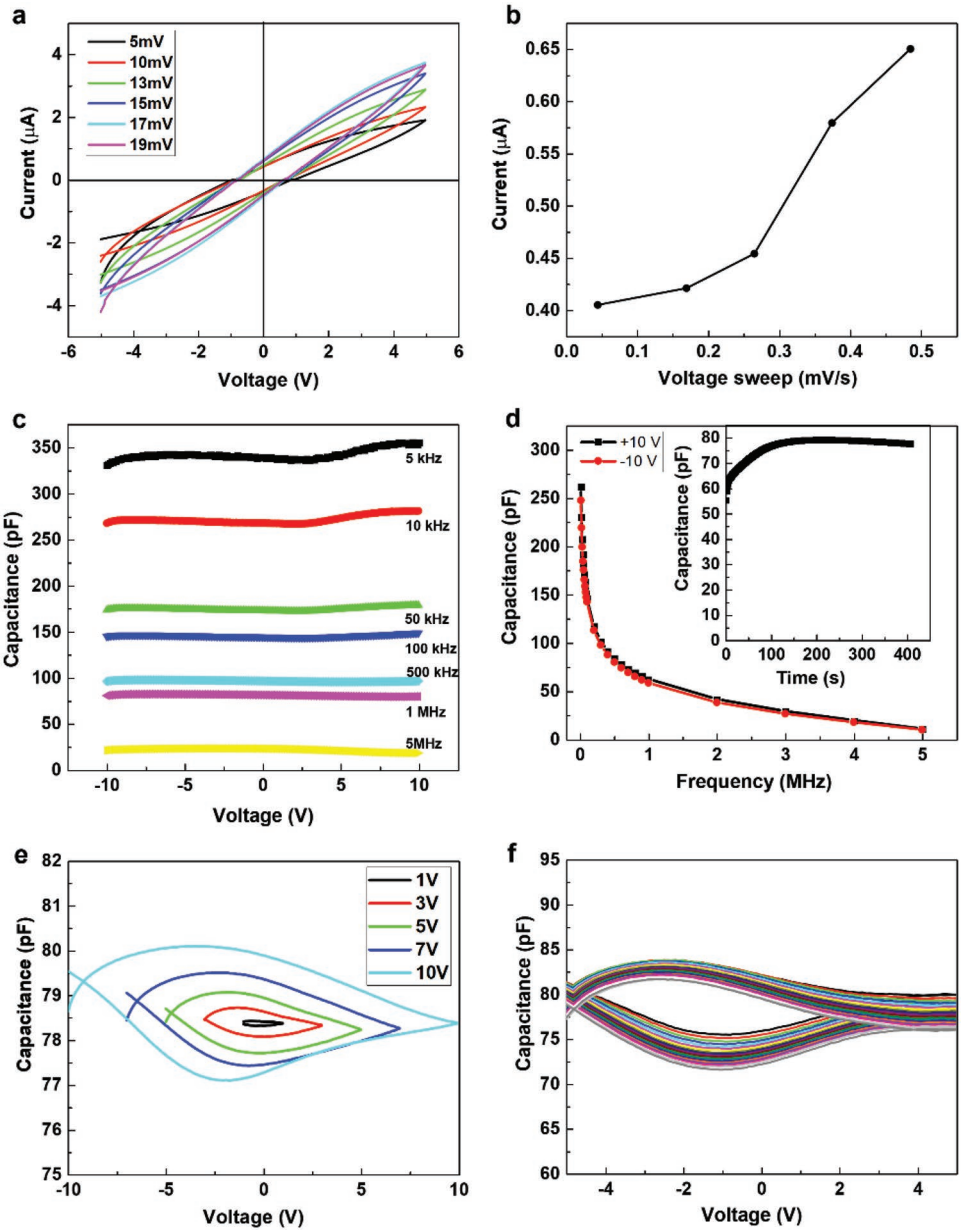

Figure 2. Electrical and capacitive characteristics of the SNF-CNT/PVA/CNT-SNF capacitor. a) Dual sweep *I*–*V* curve and b) non-zero current at zero voltage, under different sweeping voltages. c) *C*–*V* curves, between −10 V and 10 V, at selected frequencies ranging from 5 kHz to 5 MHz. d) Frequency-dependent capacitance at +10 V and −10 V. Inset shows the charging cycle of the SNF-CNT/PVA/CNT-SNF capacitor at an applied frequency of 500 kHz and DC bias of 5 V. e) *C*–*V* loop behavior with increasing applied voltage ranging from 1 V to 10 V. f) *C*–*V* curve of 20 cycles to validate the stability and reproducibility of the capacitor.

deformations of the skin, indicate its high functionality as an epidermal system for bioelectronic applications.

To investigate the electrical properties of the fabricated E-tattoo capacitor, the *I*–*V* characteristics were measured using a probe station system under different sweep voltages (*V*s) (**Figure 2**a). The dual sweep *I*–*V* curves exhibited a capacitive behavior with a non-zero crossing and hysteresis behavior, similar to the characteristics shown by previously reported biopolymer-based devices.[16] The capacitive effect is mainly attributed to the accumulation of a large number of positive and negative charge carriers at the interface between the CNT electrode layer and the PVANF layer.[17] The increased *I* level for the faster *V* scan rates implies a reduced electrical resistance. Furthermore, the areas under the *I*–*V* curves that qualitatively signify the capacitance (*C*s) of the device dwindle as the sweeping *V*s is increased (Figure 2b). This result can be attributed to the high energy loss due to the reduction in the stored charge density with the increasing sweeping rate.[18]

The *C*–*V* and capacitance–time (*C*–*t*) characteristics were measured using a semiconductor parameter analyzer. For all the measurements, *V* was applied at the top CNT/SNF layer, while the bottom CNT/SNF layer was grounded. Figure 2c

shows the frequency-dependent *C*–*V* curves (from 5 kHz to 5 MHz). We used the capacitors with an area of 1 cm^2 for all the measurements, and coaxial wires were used to minimize the effect of parasitic capacitances. Up to 500 kHz, the *C*–*V* curves showed similar behavior (Figure S6, Supporting Information), i.e., higher capacitance at +*V* with an almost same threshold voltage (≈2.7 V). Furthermore, the capacitance level decreased with the increasing frequency, due to the trapping of the positive charges more likely at the interface between the E-tattoo and the SNF-CNT electrode at a lower frequency. However, opposite behaviors were observed at frequencies greater than 500 kHz. Therefore, we selected the frequency of 500 kHz as the reading frequency for all the following capacitance measurements. Figure 2d shows the measured *C*s as a function of frequencies at a fixed DC bias *V* of ±10 V. At low frequencies, a surface electric double layer can form following the applied frequency sweep, resulting in a high *C*. However, as the frequency was increased, the responses of the mobile ion species become slower than the applied frequency, revealing a relatively lower *C*.[19] Furthermore, the inset in Figure 2d shows the charging profile of the E-tattoo capacitor, indicating that the as-fabricated capacitors can be charged quickly (<60 s) and play an important role in green and bio-friendly energy storage applications.

Figure 2e shows the dual sweep *C*–*V* curves at different *V*s (from 1 to 10 V) and an applied frequency of 500 kHz. The curves show clear hysteresis behaviors, similar to those of the previously reported metal oxide-based memory devices.[20] The loop areas are enlarged as the magnitude of *V*s and *C* values are increased, implying that our device platform can be used as a capacitance-based memory device. To validate the reproducibility and stability of the SNF-CNT/PVA/CNT-SNF E-tattoo capacitor, the dual sweep *C*–*V* measurements were conducted on five different samples for 20 cycles. As shown in Figure 2f, the deviation in *C* values is less than 2% at a DC bias *V* of 5 V, indicating a negligible change in the electrical performance.

To investigate the effects of temperature on the device performance, we obtained the *C*–*V* curves at three different temperatures (20, 80 and 160 °C), as shown in **Figure 3**a–c. Five different frequencies (f = 5, 10, 50, 100, and 500 kHz) were used for sweeping the DC bias voltage from +4 V to –4 V. The *C* values continuously dropped and reached the minimum value at –0.9 V, and then increased afterward. Notably, the rate of *C* change decreased as the applied frequency was increased. Furthermore, distinct regions of accumulation, depletion, and inversion were observed, similar to those previously reported for Al_2O_3/WSe_2 metal-oxide semiconductor-based capacitors.[21] The observed inversion suggests the feasibility of obtaining a

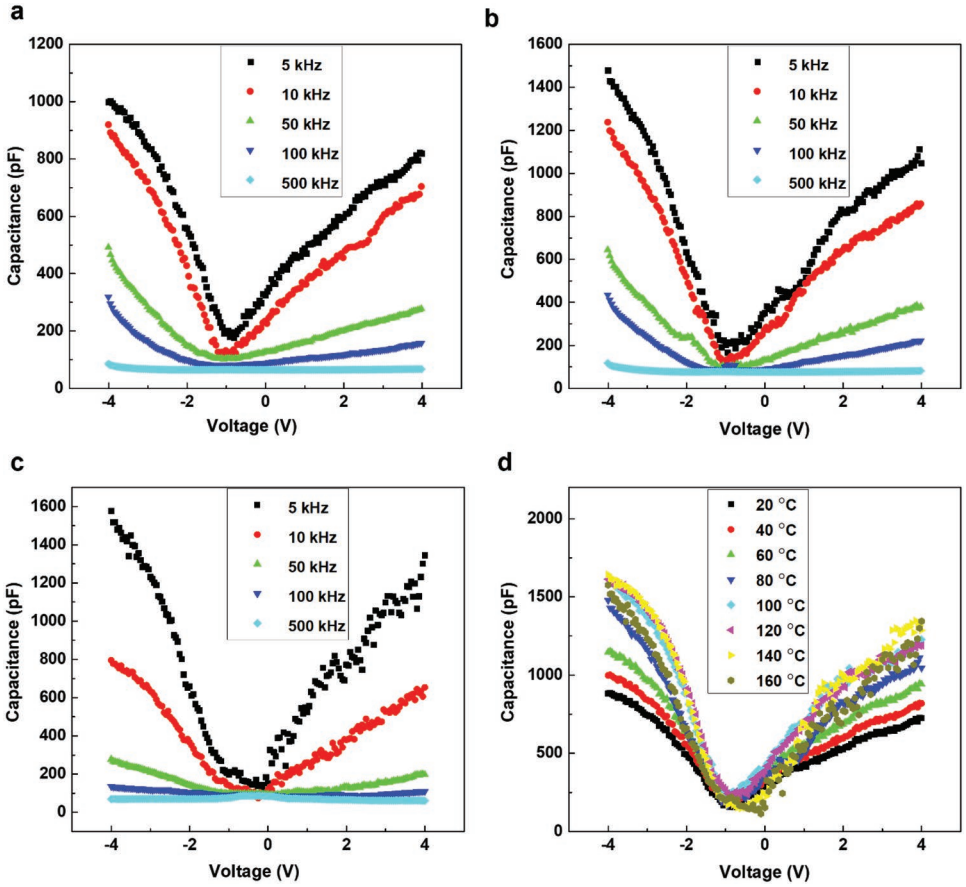

Figure 3. Temperature-dependent capacitive characteristics of the SNF-CNT/PVA/CNT-SNF capacitor. Variations in the *C*–*V* curve at a) room temperature (≈20 °C), b) 80 °C, and c) 160 °C, with an applied frequency ranging from 5 to 500 kHz. c) Temperature dependent *C*–*V* curve at 5 kHz applied frequency.

high-quality CNT/PVA interface. It should be noted that the *C* at the inversion state is lower than the maximum *C*, suggesting that some of the minority carriers in the inversion layer cannot respond at a DC bias of +4 V. This non-responsiveness of the charge carriers may be ascribed to the presence of more defects across the interface. However, a more systematic investigation is required to understand its origin. Additionally, the *C* decreases as the applied frequency is increased, because the generation rate of holes is sufficiently fast to follow the applied AC voltage (V_{ac}) modulation at lower frequencies and a given temperature. In contrast, the minority carriers in the inversion layer cannot follow the external V_{ac} modulation at higher frequencies. Further, the resistive effects induce a downshift in the *C* with the increasing frequency. In the E-tattoo capacitor, thermal energy can stimulate charge generation, resulting in an enhanced *C* of the device. The *C*–*V* curves measured at 80 and 160 °C indicate that the *C*s at all the frequencies increases at high temperatures because of the increased charge generation (Figure 3b,c). Figure 3d depicts the *C*–*V* curves measured at different temperatures (Figure S7, Supporting Information) and an applied frequency of 5 kHz. These *C*–*V* curves clearly evidence the increase in charge generation with increasing temperature. However, it should be noted that the *C* of the E-tattoo capacitor degrades at a temperature above 160 °C.

The change in *C* induced by mechanical deformations opens a way to apply the E-tattoo capacitor for monitoring physical activities of humans. To assess the activity monitoring capability of the fabricated E-tattoo, the E-tattoo capacitor device was placed on a polyimide substrate, and a mechanical force was applied to bend the device. After bending, the increase in the C_{bend}/C_{plat} ratio of the *C* values for the bended (C_{bend}) and plate-type devices (C_{plat}) were recorded. At a bending radius of 8 mm, the C_{bend}/C_{plat} ratio was ≈1.5. However, when we reduced the bending radii to 5 and 2 mm, the corresponding C_{bend}/C_{plat} ratios increased to ≈2.8 and ≈3.7, respectively. This bending-radii-dependent increase in the C_{bend}/C_{plat} ratio was due to the compression of the air gap in the dielectric layer. Notably, the increase in the C_{bend}/C_{plat} ratio was twofold when the bending radius was reduced from 8 to 5 mm. However, the increment in the ratio when the bending radius was reduced to 2 mm was comparatively lower than that obtained when the bending radius was reduced to 5 mm. The change in the capacitance have a strong dependence on the amount of axial bending of the capacitor due to the change in gap between the electrodes.[22] The relative change in the capacitance ($\Delta C/C_0$) is related to the mechanical strain ($\Delta l/l$) by the gauge factor (GF) that can be calculated by the following equation[22]

$$GF = \frac{\Delta C / C_0}{\Delta l / l} \tag{1}$$

where C_0 and l are the initial capacitance and length, respectively. The GF for 8, 5, and 2 mm bending radius was estimated to be ≈1.55 ± 0.23, 3.48 ± 0.18, and 1.68 ± 0.15, respectively. This discrepancy can be explained as follows: with the increasing bending angle, air gradually escapes from the interspace of the NF network, resulting in an increased *C*; then, the electrode layer comes in contact with the dielectric layer, and the rate of *C* increment reduces. The bending deformation is accommodated in the porous structure of the nanofibers, thereby reducing the inner stress between individual fibers.[23] Based on the mechanical stability of the E-tattoo capacitor device, the results were reproduced even after operating the device for 10 cycles. Furthermore, the GF was also quite stable even after 15 consecutive measurements (Figure S8, Supporting Information)

With capabilities for acting as a heater, conductor, and drug-delivery patch, our ultrathin E-tattoo platform can be applied as a TENG to convert mechanical touch to electronic energy.[2b] Especially, the SNF-based E-tattoo exhibits a remarkable conversion performance to bare skin touching, indicating that no additional counterpart material is required to obtain a reliable electrical performance, and the E-tattoo-based TENG is suitable for daily life use.[7d,24] As shown in **Figure 4**d, we connected an E-tattoo capacitor to an E-tattoo-based TENG through a rectifier. A human finger repeatedly touched the TENG with a frequency of 2 Hz and a force of 5 N. Interactions between the bare skin and the E-tattoo create electrical charges on the SNF surface.[25] When the bare finger touches the SNF, opposite charges are induced on the skin and SNF surfaces. When the finger travels away from the SNF surface, the generated charges cannot be compensated for, resulting in positive charges on the CNT layer, thereby leading to a notable open circuit voltage (V_{oc}) and a current in the circuit,[25]

$$V_{oc} = -\frac{\sigma A}{2C_0} \tag{2}$$

where σ is the produced charge on the nanofiber surface, *A* is the effective contact area, and C_0 is the E-skin capacitance. By increasing the distance between the finger and the E-tattoo, the negative charges on the tattoo are completely shielded from the positive charges created on the CNT electrode, resulting in no Voc. Electrons flow from the ground to the CNT electrode when the finger is pressed against the E-tattoo again, neutralizing the positive charges generated on the CNT electrode. The generated charges were stored in the connected capacitor through the rectifier. For 200 times touching, a voltage of ≈0.23 V could be obtained from the charged E-tattoo capacitor, and the capacitor could be charged further even after obtaining this much voltage from it. Although we used a breadboard because of the rectifier (Figure S9, Supporting Information), the experimental result revealed that our E-tattoo platform can act as an energy source as well as an energy storing device. Thus, the fabricated E-tattoo is feasible for an ultrathin electronic circuit, on which two or more components are integrated.

Additionally, to investigate the breathability, we evaluated the WVTR of the E-tattoo capacitor. Small glass bottles containing 300 mg of water were sealed with various membranes: no membrane, a single SNF/CNT layer (25 µm-thick), a SNF/CNT/PVANF/CNT/SNF capacitor (55 µm-thick), a commercial band-aid (150 µm-thick), and PDMS (400 µm-thick) (Figure S10, Supporting Information). To eliminate the effect of thickness, the WVTR can be normalized to film thickness *l* in order to obtain the particular water vapor transmission rate ($l \times$ WVTR).[26] The water loss was regularly recorded at a temperature of 25 °C and humidity of 58% (Figure 4e). Although the WVTR for the E-tattoo capacitor (115.04 g m^{-2} d^{-1}) was lower than that for the single SNF/CNT layer (261.32 g m^{-2} d^{-1}) because of the

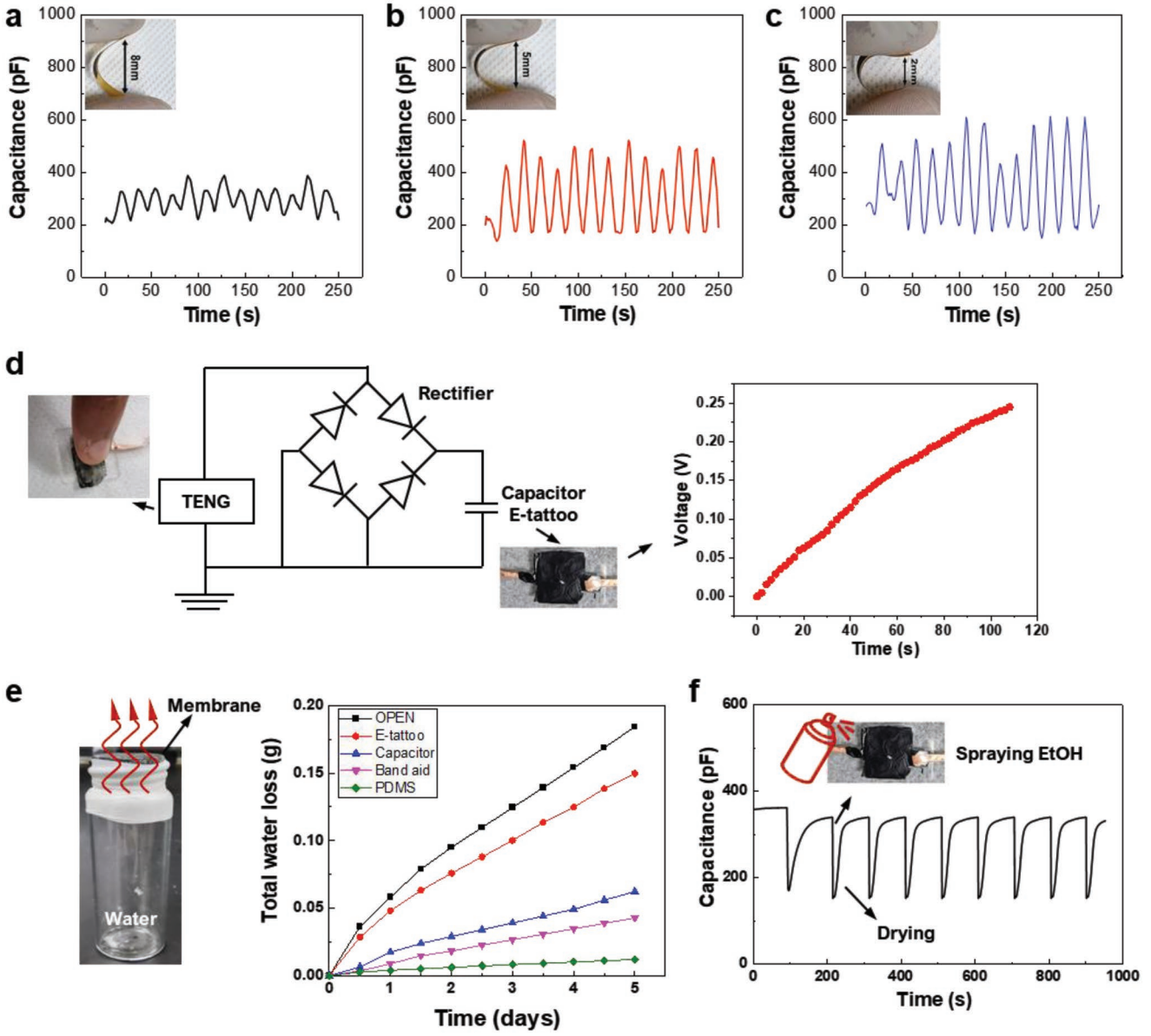

Figure 4. Demonstrating the multifunctionality of the SNF-CNT/PVA/CNT-SNF capacitor. *C*–*t* curve showing the flexibility of the capacitor at a) 8 mm, b) 5 mm, and c) 2 mm bending radii. d) Charging of the capacitor using a skin actuated TENG after rectification by a full-wave bridge rectifier. e) Comparison of water vapor permeability between an open vial and a vial sealed with a silk-CNT-based E-tattoo, SNF-CNT/PVA/CNT-SNF capacitor, commercial medical tape, and PDMS thin film. f) Inset shows the schematic illustration for ethanol sensing and the variation in *C*–*t* under ethanol exposure. The stability and reproducibility were demonstrated via repetitive measurements (≈10 cycles).

densely packed CNTs, it showed a higher WVTR than that of the commercial band-aid (Figure S11, Supporting Information). With the advantage of lightness, the breathability of the E-tattoo is expected to facilitate its imperceptible and comfortable applications in daily life. A major application of the breathable and permeable E-tattoo capacitor is volatile organic compound monitoring. Especially, sensing EtOH is important for automobile (against drunk driving) and chemical (gas leakage) industries.[10] We measured the change in *C* values when EtOH was sprayed on the SNF-CNT/PVANF/CNT-SNF film and subsequently dried at 80 °C. The *C* value instantly decreased to half of its original value as EtOH was sprayed, and was then promptly recovered after drying (Figure 4f). The *C*–*t* behavior for 10 exposure–drying cycles showed the high reproducibility of our device. Due to the breathability, permeability, and biocompatibility (of the SNFs), our E-tattoo platform is suitable for on-skin electronic devices and biomedical applications.

3. Conclusion

In summary, we demonstrated a highly breathable and biocompatible skin attachable capacitor fabricated using silk-CNT-based electrodes and a PVANF dielectric layer. The

ultrathin E-tattoo capacitor (≈20 μm) with a low sheet resistance (200 Ω/□) and negligible changes in electrical resistance can be a potential alternative in flexible device electronics. The detailed electrical characteristics of this capacitor demonstrate that the capacitive effect can be mainly attributed to the accumulation of a large number of positive and negative charge carriers at the interface between the CNT electrode layer and the PVANF layer. This epidermal capacitor showed a better water vapor transmission rate as well as a high sensitivity against mechanical deformation and ethanol exposure. This unique device is anticipated to open avenues for many future applications, such as conformal wearable medical devices, intelligent robotics and prostheses, selective gas sensing, and healthcare monitoring.

4. Experimental Section

Preparation of Silk Protein Solution: To extract the silk fibroin, fresh *Bombyx mori* cocoons were sliced into tiny pieces and boiled for 30 min in an aqueous solution of 0.02 M sodium carbonate (Na_2CO_3). Sericin was removed from the cocoons by boiling, then washed many times in distilled water before being dried for 24 h. Afterward, a 9.3 M lithium bromide (LiBr) solution was used to dissolve the dried silk fibroin and the mixture was then incubated for 4 h at 60 °C, resulting in a 20 wt.% solution. A dialysis membrane (Cellu-Sep T1, Membrane Filtration Products, molecular weight cutoff = 3.5 k) was used to dialyze the resulting silk solution against distilled water at room temperature for 48 h. The dialysate was centrifuged twice for 20 min at 4 °C and 9000 revolutions per minute to eliminate contaminants. The final concentration of the aqueous silk fibroin solution was ≈8 wt.%.

Electrospinning: First, poly(ethylene oxide) (PEO) (M_w ≈900 000, Sigma–Aldrich) was added to the as-prepared silk solution to prepare a mixture with an enhanced viscosity, appropriate for electrospinning, which was used to create the SNFs. The main solution was prepared by combining the silk solution and the PEO solution with 5 wt.% at a ratio of 1:1, and thoroughly mixing them using a vortex mixer. The electrospinning machine was equipped with a syringe that was filled with the silk/PEO solution to create the SNF network. The collector consisted of a sheet of aluminum foil on which glass slides had been affixed using a Scotch tape. The flow velocity of the silk/PEO solution was adjusted to 10 μL min^{-1}, and the distance between the tip and the collector was kept constant at 15 cm. The electrospinning was performed for 60 min at a voltage of 20 kV maintained between the 23 G nozzle tip and the collector. After the SNF/glass substrate samples were collected, they were treated with methanol to render the SNFs water-insoluble and to facilitate the removal of the used PEO.

Subsequently, PVA (M_w ≈40000, Sigma–Aldrich) was used to fabricate a dielectric layer. For obtaining a homogenous solution, 15 mg of PVA was dissolved in 100 mL of water at 80 °C for 2 h under continuously stirring by a magnetic stirrer (2000 rpm). Then, the final solution was electrospun on a glass slide affixed to a collection plate using a Scotch tape. A 15 cm separation between the nozzle and the collector was maintained, and a 5 μL min^{-1} flow rate was adopted. Throughout the 60 mins of electrospinning, a voltage of 20 kV was maintained between the 23 G nozzle tip and the collector. The produced electrospun PVA fiber mat was scraped from the glass slides and utilized as a middle sandwich layer.

CNT Ink Preparation: To disperse the single-wall CNTs (Sigma–Aldrich) thoroughly in methanol, sodium lauryl sulfate (≈5 mg mL^{-1}) was first dissolved in methanol, and then 1 mg mL^{-1} of CNT was added to the solution, which was then ultrasonically treated for 2 h. In order to prepare a viscous solution, 3 mg mL^{-1} of PEO was added, followed by mixing for 18 h on a stirrer plate.

Fabrication of CNT-Functionalized SNF E-Tattoos: The CNT ink was applied to the SNF network/glass substrate using a paintbrush and allowed to dry for 1 h. The membrane was then separated from its substrate by peeling it away. The freestanding membrane was then sliced into small squares (≈1 cm^2).

Fabrication of SNF-CNT/PVANF/CNT-SNF Biopolymer Capacitors: The PVA nanofiber mats were first sliced into square shapes (≈1 cm^2) and used as a sandwich layer. In this case, a square-shaped PVA fiber mat was mechanically pressed on top of the CNT-SNF tattoo after spraying a small amount of ethanol on it. To synthesize a whole biocompatible capacitor, a similar method was employed to attach the SNF-CNT layer permanently on the top. fine copper wires (Nilaco, CU111267) were attached to the CNT surface using silver paste to measure the electrical properties.

Characterizations: Field emission scanning electron microscope (JSM6700F, JEOL, Japan) and FTIR (Nicolet 50, Thermo fisher) spectroscopy were used to examine the morphological and structural characteristics of the E-tattoo stickers. A Keithley 4200A-SCS system was used for the *I–V* and capacitance measurements. The flexibility of the E-tattoos were evaluated by attaching them to pigskin and measuring their electrical characteristics. The *C–V* readings were recorded using a Keithley 4200A-SCS system by applying a combined DC and modulation AC voltage (V_{ac}) of 100 mV at frequencies ranging from 5 kHz to 5 MHz.

Supporting Information

Supporting Information is available from the Wiley Online Library or from the author.

Acknowledgements

The authors acknowledge supports from the National Research Foundation (NRF) of Korea (no. 2019R1A2C2088615) and the Rural Development Administration (PJ016130, Research Program for Agricultural Science and Technology Development of the National Academy of Agricultural Science).

Conflict of Interest

The authors declare no conflict of interest.

Data Availability Statement

Research data are not shared.

Keywords

capacitor, electronic tattoo, energy storage, on-skin sensing, silk nanofiber, ultrathin electronics

Received: September 28, 2022
Revised: November 17, 2022
Published online:

[1] a) F. Stauffer, M. Thielen, C. Sauter, S. Chardonnens, S. Bachmann, K. Tybrandt, C. Peters, C. Hierold, J. Voros, *Adv. Healthcare Mater.* **2018**, *7*, 1700994; b) T. Kim, J. Park, J. Sohn, D. Cho, S. Jeon, *ACS Nano* **2016**, *10*, 4770.

[2] a) N. Gogurla, S. Kim, *Adv. Energy Mater.* **2021**, *11*, 2100801; b) N. Gogurla, Y. Kim, S. Cho, J. Kim, S. Kim, *Adv. Mater.* **2021**, *33*, 2008308.

[3] a) K. He, Z. Liu, C. Wan, Y. Jiang, T. Wang, M. Wang, F. Zhang, Y. Liu, L. Pan, M. Xiao, H. Yang, X. Chen, *Adv. Mater.* **2020**, *32*, 2001130; b) Z. Li, X. Wu, X. Jiang, B. Shen, Z. Teng, D. Sun, G. Fu, Y. Tang, *Adv. Pow. Mater.* **2022**, *1*, 100020.

[4] a) D. H. Kim, N. Lu, R. Ma, Y. S. Kim, R. H. Kim, S. Wang, J. Wu, S. M. Won, H. Tao, A. Islam, K. J. Yu, T. I. Kim, R. Chowdhury, M. Ying, L. Xu, M. Li, H. J. Chung, H. Keum, M. McCormick, P. Liu, Y. W. Zhang, F. G. Omenetto, Y. Huang, T. Coleman, J. A. Rogers, *Science* **2011**, *333*, 838; b) K. Sim, Z. Rao, Z. Zou, F. Ershad, J. Lei, A. Thukral, J. Chen, Q. A. Huang, J. Xiao, C. Yu, *Sci. Adv.* **2019**, *5*, eaav9653.

[5] A. Campana, T. Cramer, D. T. Simon, M. Berggren, F. Biscarini, *Adv. Mater.* **2014**, *26*, 3874.

[6] S. Yang, Y. C. Chen, L. Nicolini, P. Pasupathy, J. Sacks, B. Su, R. Yang, D. Sanchez, Y. F. Chang, P. Wang, D. Schnyer, D. Neikirk, N. Lu, *Adv. Mater.* **2015**, *27*, 6423.

[7] a) K. Min, S. Kim, S. Kim, *Proc Natl Acad Sci U S A* **2017**, *114*, 6185; b) S. Kim, A. N. Mitropoulos, J. D. Spitzberg, D. L. Kaplan, F. G. Omenetto, *Opt. Express* **2013**, *21*, 8897; c) K. Min, S. Kim, S. Kim, *Sci. Rep.* **2018**, *8*, 9598; d) N. Gogurla, B. Roy, J. Y. Park, S. Kim, *Nano Energy* **2019**, *62*, 674.

[8] a) X. Lu, Y. Zhu, R. Bai, Z. Wu, W. Qian, L. Yang, R. Cai, H. Yan, T. Li, V. Pandey, Y. Liu, P. E. Lobie, C. Chen, T. Zhu, *Nat. Nanotechnol.* **2019**, *14*, 719; b) K. Kim, M. J. Kim, D. W. Kim, S. Y. Kim, S. Park, C. B. Park, *Nat. Commun.* **2020**, *11*, 119; c) S. Y. Kwak, T. T. S. Lew, C. J. Sweeney, V. B. Koman, M. H. Wong, K. B. Tatarev, K. D. Snell, J. S. Seo, N. H. Chua, M. S. Strano, *Nat. Nanotechnol.* **2019**, *14*, 447; d) R. Soni, S. R. Joshi, M. Karmacharya, H. Min, S. K. Kim, S. Kumar, G. H. Kim, Y. K. Cho, C. Y. Lee, *ACS Appl. Nano Mater.* **2021**, *4*, 8491.

[9] J. C. Yang, J. Mun, S. Y. Kwon, S. Park, Z. Bao, S. Park, *Adv. Mater.* **2019**, *31*, 1904765.

[10] a) P. Cao, Z. Yang, S. T. Navale, S. Han, X. Liu, W. Liu, Y. Lu, F. J. Stadler, D. Zhu, *Sens. Actuators, B* **2019**, *298*, 126850; b) E. Spagnoli, S. Krik, B. Fabbri, M. Valt, M. Ardit, A. Gaiardo, L. Vanzetti, M. D. Ciana, V. Cristino, G. Vola, S. Caramori, C. Malagù, V. Guidi, *Sens. Actuators, B* **2021**, *347*, 130593.

[11] D. Yu, M. Humar, K. Meserve, R. C. Bailey, S. N. Chormaic, F. Vollmer, *Nat. Rev. Methods Primers* **2021**, *1*, 83.

[12] a) J. Rao, Z. Chen, D. Zhao, Y. Yin, X. Wang, F. Yi, *Sensors* **2019**, *19*, 2763; b) Y. Chen, Z. Gao, F. Zhang, Z. Wen, X. Sun, *Exploration* **2022**, *2*, 20210112.

[13] a) Z. Ma, Q. Huan, Q. Xu, Q. Zhuang, X. Zhao, Y. yang, H. Qiu, Z. Yang, C. Wang, Y. Chai, Z. Zheng, *Nat. Mater.* **2021**, *20*, 859; b) F. Chen, Q. Huang, Z. Zheng, *Small Struct.* **2022**, *3*, 2100135; c) S. Lee, S. Franklin, F. A. Hassani, T. Yokota, M. O. G. Nayeem, Y. Wang, R. Leib, G. Cheng, D. W. Franklin, T. Someya, *Science* **2020**, *370*, 966; d) A. Miyamoto, S. Lee, N. F. Cooray, S. Lee, M. Mori, N. Matsuhisa, H. Jin, L. Yoda, T. Yokota, A. Itoh, M. Sekino, H. Kawasaki, T. Ebihara, M. Amagai, T. Someya, *Nat. Nanotechnol.* **2017**, *12*, 907; e) Q. Huang, Z. Zheng, *ACS Nano* **2022**, *16*, 15537; f) Q. Zhuang, Z. Ma, Y. Gao, Y. Zhang, S. Wang, X. Lu, H. Hu, C. Cheung, Q. Huang, Z. Zheng, *Adv. Funct. Mater.* **2021**, *31*, 2105587.

[14] H. Liu, W. Wei, L. Zhang, J. Xiao, J. Pan, Q. Wu, S. Ma, H. Dong, L. Yu, W. Yang, D. Wei, H. Ouyang, Y. Liu, *Adv. Funct. Mater.* **2021**, *31*, 2104088.

[15] S. A. Girei, S. P. Thomas, M. A. Atieh, K. Mezghani, S. K. De, S. Bandyopadhyay, A. A. Juhani, *J. Thermoplast. Compos. Mater.* **2011**, *25*, 333.

[16] a) Y. Zeng, B. Sun, H. Y. Yu, X. Wang, H. Peng, Y. Chen, S. Zhu, S. Mao, W. Hou, *Mater. Today Chem.* **2019**, *13*, 18; b) B. Guo, B. Sun, W. Hou, Y. Chen, S. Zhu, S. Mao, L. Zheng, M. Lei, B. Li, G. Fu, *RSC Adv.* **2019**, *9*, 12436; c) S. Mao, B. Sun, T. Yu, W. Mao, S. Zhu, Y. Ni, H. Wang, Y. Zhao, Y. Chen, *New J. Chem.* **2019**, *43*, 9634.

[17] X. Guo, L. Huang, X. Zhou, Q. Chang, C. Cao, G. Xiao, W. Shi, *Adv. Funct. Mater.* **2020**, *30*, 2003635.

[18] M. M. Nofal, J. M. Hadi, S. B. Aziz, M. A. Brza, A. Asnawi, E. M. A. Dannoun, A. M. Abdullah, M. F. Z. Kadir, *Materials* **2021**, *14*, 4859.

[19] K. Keum, J. Eom, J. H. Lee, J. S. Heo, S. K. Park, Y. H. Kim, *Nano Energy* **2021**, *79*, 105479.

[20] a) J. Wang, M. Schitko, G. Mussler, D. Grützmacher, D. Weiss, *Phys. Status Solidi* **2019**, *256*, 1800624; b) W. H. Qian, X. F. Cheng, Y. Y. Zhao, J. Zhou, J. H. He, H. Li, Q. F. Xu, N. J. Li, D. Y. Chen, J. M. Lu, *Adv. Mater.* **2019**, *31*, 1806424.

[21] M. Kang, H. I. Yang, W. Choi, *J. Phys. D: Appl. Phys.* **2020**, *53*, 32LT01.

[22] a) A. Bessonov, M. Kirikova, S. Haque, I. Gartseev, *Sens. Actuators* **2014**, *206*, 75; b) C. F. Hu, J. Y. Wang, Y. C. Liu, M. H. Tsai, W. Fang, *Nanotechnology* **2013**, *24*, 444006.

[23] S. Lee, A. Reuveny, J. Reeder, S. Lee, H. Jin, Q. Liu, T. Yokota, T. Sekitani, T. Isoyama, Y. Abe, Z. Suo, T. Someya, *Nat. Nanotechnol* **2016**, *11*, 472.

[24] A. Pratap, N. Gogurla, S. Kim, *ACS Appl. Electron. Mater.* **2022**, *4*, 1124.

[25] a) J. Luo, Z. L. Wang, *EcoMat.* **2020**, *2*, e12059; b) S. Chao, H. Quyang, D. Jiang, Y. Fan, Z. Li, *EcoMat.* **2020**, *3*, e12072.

[26] G. C. Lainioti, G. Bounos, G. A. Voyiatzis, J. K. Kallitsis, *Polymers* **2016**, *8*, 190.